Removal of Methylene blue from aqueous solution by Montmorillonite/$ZnFe_2O_4$ composite with Magnetic and Photo-induced recyclable performance

R.Chitradevi[ab],E.Vaishnavi[b], K. Poonkodi[c], V.Anitha[b]Subramanian Rajalakshmi[d]and P. N. Magudeswaran[e]*

[a]Research and Development Centre, Bharathiar University, Coimbatore – 641 046, Tamil Nadu, India.
[b]Department of Chemistry, Sri GVG Visalakshi College for Women, Udumalpet – 642128, Tamil Nadu, India.
[c]Department of Chemistry, Sri GVG Visalakshi College for Women, Udumalpet– 642128, Tamil Nadu, India.
[d]Department of Chemistry, Erode Arts and Science College (Autonomous), Erode 638112, India.
[e]Hindustan College of Engineering and Technology, Coimbatore – 641050, Tamil Nadu, India.

***Corresponding author:**

Dr. P.N. Magudeswaran,
Dean Academics,
Hindustan College of Engineering and Technology,
Coimbatore – 641050, Tamil Nadu, India.
E-mail: magudeswaran2021@gmail.com. Ph. +91-9842009872

Abstract

Stacked layer structure of $ZnFe_2O_4$/Montmorillonite K10nanocomposite was prepared by co-precipitation method and using eco-friendly adsorbent for the removal of MB dye from aqueous solution. The resultant adsorbent was recycled and reused by sunlight illumination due to the photocatalytic properties of $ZnFe_2O_4$.The magnetic property of nanocomposite shows high magnetic saturation with super-paramagnetic nature, which makes an additional use for adsorbent separated from the dye suspension.Batch experiments were carried out under different conditions of initial dye concentration and contact time to investigate the adsorption capacities of $ZnFe_2O_4$/MMTK10 nanocomposite towards MB.The adsorption isotherms were used to fit the experimental data. The obtained experimental results precisely fitted into Langmuir isothermwith maximum adsorption capacities of 218.3 mg g^{-1} for MB. Also, pseudo-first-order andpseudo-second-order kinetic models were applied, and the experimental data fitted the pseudo-second ordermodel (R^2 = 0.9995). The combined magnetic and photo-induced recycling properties of$ZnFe_2O_4$/MMTK10 nanocomposite could be a promising approach to facilitate as adsorbent for the removal of MB dyes from aqueous solution.

Keywords: Montmorillonite, composite, adsorbent, adsorption, kinetics, $ZnFe_2O_4$/MMTK10.

1. Introduction

Textile dyeing is the main source of polluting aspects of the global industry, devastating the environment, leading to severe health hazards [1]. The colourful dyes used in clothes, faded our natural earth by production of more than 1 00 000 types of dyes in the market, and each year, about 7 00 000 tons of dyes are prepared leading to severe water pollution [2-4]. The dyeing industry utilises around 93 billion cubic meters of water annually. Intensive attention towards the necessity of zero water discharge from industries into the river has to be created. The development of various treatment processes including physical separation, chemical oxidation and biological degradation have been widely investigated to remove dyes from wastewaters. Traditionally, many methods have been practiced to remove the dyes from contaminated waters, which includes adsorption, membrane filtration, distillation,coagulation, oxidation, ion exchange, electrolysis, precipitation, photochemical degradation, and reverse osmosis [5-15].Apart from the aforementioned process, adsorption can be thought to be the most effective process for the treatment of wastewater due to its low-cost and ease of operation as well as greater efficiency [16].

Adsorbent used in the adsorption process plays a vital role in the removal of dyes from wastewater. Many kinds of adsorbents were reported, for instance, activated carbon, zeolite, fly ash, clay, chitosan and by-products from juice processing [17-21]. The efficacy of the activated carbons offers an attractive option for the efficient removal of various organic contaminants from water due to their high surface area and porous structure. In contrast, their practice use on a large scale is limited by process engineering difficulties.

In this perspective, considering the significance of non-conventional low-cost adsorbents for dye removal, clay minerals have been often used in the remove of organic dyes [22-24], due to their cost-effectiveness, process simplicity, high surface area, commercial availability, good efficiency, and eco-friendly nature [25, 26]. Nevertheless, these adsorbents suffer from common operational issues

such as reusability, stability in long-duration operations, and dye leaching after saturation. Clays were incorporated with different materials to overcome these operational issues. In this way, montmorillonite (MMT) clay improves the dye removal at a larger scale by enriching with nanoparticles.

In recent research, nanoparticle adsorbents, such as MnO_2, Fe_3O_4, TiO_2, $MnFe_2O_4$, MFe_2O_4 [27-31], etc., gain widespread recognition as a result of their smaller size, high surface-area-to-volume ratio and unique morphology. It is worthwhile to mention that nanoparticle adsorbents enhance the removal of metal ions and organic contamination from aqueous solutions. Moreover, for such an application, it is essential to use a method of purification that should be free from secondary pollution, materials that can be recycled and easily used on an industrial scale [32]. Magnetic separation is considered as a quick and effective technique for separating magnetic particles. It has been used for many applications in biochemistry, analytical chemistry, and mining ores. Recently, considerable attention has been focused on the development of magnetic separation to solve environmental problems [33-35]. Herein, to further stimulate the tendency of absorption a new kind of magnetic adsorbent, montmorillonite K10/$ZnFe_2O_4$ nanocomposite, was developed for removal of dye in aqueous solution. Therefore, combinatorial methods of fabricating clay materials and magnetic particles can be promising adsorbent and open new possibilities for the achievement of desirable adsorption and effective magnetic separation.

In this paper, $ZnFe_2O_4$/Montmorillonite K10 (MMT K10) nanocomposite prepared by hydrothermal method and used for removal of methylene blue (MB). The purpose of this work was to composite the MMT K10 with $ZnFe_2O_4$ and to compare the adsorption capacity of $ZnFe_2O_4$ and $ZnFe_2O_4$/MMT K10 nanocomposite. The adsorption kinetics and isotherms were further studied by fitting the experimental data with different models. In addition, the dye adsorbed $ZnFe_2O_4$/MMT K10 nanocomposite can be reused and regenerated by means of photo induced process under sunlight irradiation. Interestingly, this method impresses very well the process of solvent extraction. Compared to conventional solvent extraction, the photo-induce regeneration of $ZnFe_2O_4$/MMT K10

nanocomposite has a simple green system and avoids the use of toxic solvent. Therefore, this study is believed to provide a new system for effective wastewater treatment.

2. Experimental method

2.1. Materials

Iron (III) nitrate nonahydrate ($Fe(NO_3)_3.9H_2O$, 99%), zinc nitrate hexahydrate $Zn(NO_3)_2.6H_2O$, 99%), and sodium hydroxide (NaOH) were purchased from Merck Co. Montmorillonite K10 (Sigma-Aldrich) and methylene blue (MB) (Sigma-Aldrich, $C_{16}H_{18}ClN_3S.3H_2O$, 373.9 g mol^{-1}) were used as received without any further purification.

2.2. Preparation of $ZnFe_2O_4$/montmorillonite K10 nanocomposite

Magnetic $ZnFe_2O_4$/MMT K10 nanocomposite was prepared by a co-precipitation method [36]. 1 mg of MMT K10 was added into 50 ml deionized water with ultrasonication to form a uniform dispersion. 0.1 M of $Zn(NO_3)_2.6H_2O$ and 0.2 M of $Fe(NO_3)_2.9H_2O$ were added into 30 ml of deionized water, stirred for 10 min and added slowly into the above solution under stirring. The pH was adjusted to pH 9-10 using NaOH (3 mol L^{-1}) solution and the solution was stirred for 5 h at 80 °C. After completing the reaction, the resulting precipitate sample was filtered and washed with deionized water and ethanol for a several times, dried under hot air oven at 80 ºC for 12 h. The final product was annealed at 500 ºC for 4 h under nitrogen atmosphere. For comparison, a similar procedure was used to prepare bare $ZnFe_2O_4$ without MMT/K10.

2.3. Characterization of $ZnFe_2O_4$/MMT K10 nanocomposite

X-ray diffraction (XRD) patterns were obtained using X-pert Pro' PAnalytical powder X-ray diffractometer with Cu Kα radiation (λ= 0.1541 nm). The functional groups on the surface of the adsorbents were identified using Fourier transform infrared (FTIR) spectrometer (Jasco FT-IR-6600) in the wavelength range of 4000–400 cm^{-1}. Sample morphologies and microstructures were characterized by scanning electron microscopy (SEM) [Carl Zeiss Σigma]. The diffuse reflectance spectra (DRS) were recorded using an UV−Vis spectrophotometer within a range of 200−800 nm.The magnetic

features of the synthesisedadsorbents were characterised using a vibrating samplemagnetometer (VSM, Princeton Measurements MicromagModel 3900); the field applied ranged from – 1T to 1T.

The surface charges and Zeta potential of $ZnFe_2O_4$/MMT K10 nanocompositewas obtained using Zeta potential analyser (Malvern).

2.4. Adsorption experiments

The adsorption characteristics of $ZnFe_2O_4$ and $ZnFe_2O_4$/MMT K10 nanocomposite towards MBwere obtained through batch adsorption experiments conducted at their different initial concentrations (from 25 to 1000 mg L^{-1}) at pH 7. A series of experiments were conducted by adding 25 mg of adsorbent to 25 ml of an aqueous solution of desired concentration containing MB followed by shaking at 60 rpm for 24 h using a rotary shaker until the equilibrium was reached.After that, the adsorbent was separated by centrifuging and filtration. The residual concentrations of MB are obtained using heights of maximum adsorption peaks of MB (662 nm) through UV-Vis analysis (Fig. 7). The equilibrium adsorption capacity (q_e) was calculated as follows[37]

$$q_e = (C_0 - C_e)\frac{V}{m} \quad \text{(Eq.1)}$$

where $q_e$represents the adsorption capacity (mg g^{-1}) at equilibrium. C_0 and C_e are the initial and equilibrium concentration (mg L^{-1}) ofdye, respectively; *V* and *m* are the volume of solution (mL) and mass of theadsorbent (g), respectively.Adsorption and kinetics experiments were performed at room temperature (25 °C) and pH 7. All the experiments were performed in triplicate. Data presented are the mean from three independent experiments and the error bars represent the standard deviation of triplicate measurements. The appropriateness of the fit was measured through correlation coefficient (R^2) values.

2.5. Kinetics experiments

The rate of adsorption and the effect of contact time on MB adsorptions were quantified through kinetic tests. Furthermore, the kinetics of MB adsorptionson $ZnFe_2O_4$ and $ZnFe_2O_4$/MMT K10 nanocompositeweretested by adding 25 mg of as-prepared $ZnFe_2O_4$ or $ZnFe_2O_4$/MMT K10

nanocomposite in 25 mL of MB (200 mg L^{-1}) at room temperature. The analytes were extracted at various time intervals and diluted 100 times before the quantifying concentrations of MB through UV-Vis analyses. The adsorbed quantity of MB/Rh B at time *t* was calculated (Eq. 2) as follows [37]:

$$q_t = (C_0 - C_t)\frac{V}{m} \text{(Eq. 2)}$$

where C_0 (mg L^{-1}) represents the initial concentration of MB C_t (mg L^{-1}) indicates the concentration of MB at time *t*.*V* (L) and m (g) represent the volume of MB solution and weight of adsorbent ($ZnFe_2O_4$/MMT K10 nanocomposite), respectively.

3. Results and discussion

3.1 Structural and morphological studies

The XRD patterns of the $ZnFe_2O_4$comparison with the $ZnFe_2O_4$/MMT K10nanocomposite is shown in Fig.1. Intense diffraction peaks of $ZnFe_2O_4$at 2θ = 30.1°, 35.5°, 43.2°, 53.3°, 57.11°, and 62.5° wereascribed to the reflection of 220, 311, 400, 422, 511, and440 planes of $ZnFe_2O_4$, which were well-indexed to the cubicspinel structure (JCPDS card no. 22-1012) [38]. No other peaks related to the impurities were detected.The diffraction peaks at 8.6°,19.5°, 34.8°, and 45.17° corresponded to MMT K10, which were well matched with the reportedspectra (JCPDS file no. 29-1498) [39, 40]. Quartz is present in MMT K10, evidenced by thepattern at 20.5°, 26.3°, 49.9°, and 59.8° [41]. Fig. 1c shows the XRD patterns of the $ZnFe_2O_4$/MMT K10 nanocomposite. All characteristic diffraction peaksof $ZnFe_2O_4$ and MMT were indexed in the XRD patterns of $ZnFe_2O_4$/MMT K10 nanocomposite, which confirmed the presenceof $ZnFe_2O_4$ within the MMT K10 clay surface. The peak of $ZnFe_2O_4$ at 35.5°, presented beside the MMT K10 35.1° (110) peak in the spectra of $ZnFe_2O_4$/MMT K10 nanocomposite, indicated that the (110) plane of $ZnFe_2O_4$/MMT K10 became more disordered than that of MMT K10 clay due to the loading of $ZnFe_2O_4$. More importantly, loading $ZnFe_2O_4$onto the MMT K10 changed the d_{001}-value from 1.02 nm to 1.22 nm, indicating that exchangeable metal ions and interlayer water molecules were replaced by $ZnFe_2O_4$which intercalated into the silicate layers of MMT K10 during the synthesis procedure [42].

Formation of the $ZnFe_2O_4$/MMT K10 nanocomposite was determined using FTIR spectroscopy. The comparison FTIR spectra with functional groups of zinc ferrite with the nanocomposite were shown in Fig.2. $ZnFe_2O_4$ exhibited two characteristic peaks at 588 and 416 cm^{-1}, which were assigned to metal−oxygen intrinsic vibrations of tetrahedral and octahedral sites in the spinel ferrite structure, respectively [43, 44]. The characteristic strong peaks at 1,031, 798 and 520 cm^{-1} of MMT K10 are assigned to the stretching of Si–O and Si—O—Al, respectively [45, 46]. The absorption bands at 3423 and 1630 cm^{-1} can be ascribed to the O—H stretching vibrations [47]. The shifting and lower intensity of the Si—O bands in the $ZnFe_2O_4$/MMT K10 nanocomposite, indicating that the Fe—O bonds may interact with the Si—O bonds on the surface of MMT K10. These results can be interpreted as being the consequence of Zn^{2+}/Fe^{3+} exchanging the Al^{3+} groups of the crystal structure of the MMT K10 clay.

The surface morphology, uniform distribution of $ZnFe_2O_4$ on the MMT K10 clay was explored using SEM and TEM (Fig.3). SEM image of the MMT K10 clay exhibited the irregular particles with agglomeration and heterogeneous sheet like structure in various sizes. For $ZnFe_2O_4$ (Fig. 3a), the aggregated nanofibrous structure with various size was clearly observed, which is due the magnetic properties of the synthesized zinc ferrite nanofibrous. The $ZnFe_2O_4$ nanofibrous have an average size of around 50 -100 nm. Fig. 3c&d shows the low and high magnification of $ZnFe_2O_4$/MMT K10 nanocomposite. The $ZnFe_2O_4$ nanofibrous were distributed over exfoliated MMT K10 layers, creating void spaces. Further, the $ZnFe_2O_4$ nanofibrous seems to be closely anchored on the surface of exfoliated MMT K10, suggesting the strong interaction between $ZnFe_2O_4$ nanofibrous and MMT K10 clay. Moreover, the nanofibrous were intensely bound to the MMT K10 clay due to the magnetic dipolar interactions among nanofibrous. The fibrous structure of $ZnFe_2O_4$ anchored nanocomposite is increase the surface area and aids the higher dye adsorption efficiency.

Fig. 3e displays the TEM image of $ZnFe_2O_4$/MMT K10 nanocomposite with the increase of amount of loaded $ZnFe_2O_4$ nanofibrous. The observed result shows that $ZnFe_2O_4$ nanofibrous were homogenously distributed on the surfaces of MMT K10 clay with less agglomeration. In the EDX

analysis (Fig. 3f) of nanocomposite displays the presence of all elements of MMT K10 and $ZnFe_2O_4$. Also, the absence of exchangeable metal ions and reduction in the Al and Si content in the nanocomposite indicates that $ZnFe_2O_4$ nanofibrous was successfully intercalated into the MMT K10 layers and simultaneously anchored on the surface of MMT K10 layers. This implies that $ZnFe_2O_4$/MMT K10 nanocomposite can be provide more surface area and enhance the dye adsorption capacity.

3.2. Optical and magnetic properties

The optical absorption properties of $ZnFe_2O_4$ and $ZnFe_2O_4$/MMT K10 nanocomposite were demonstrated in Fig.4a. UV-DRS spectra of $ZnFe_2O_4$/MMT K10 nanocomposite exhibited the continuous broad absorption (350 and 450 nm) with higher intensity than bare $ZnFe_2O_4$. The absorption intensity of $ZnFe_2O_4$/MMT K10 nanocomposite was enhanced in the visible light region, suggesting that the oxygen vacancies having a new donor energy level, which give the semiconductor with narrow band gap energy to enhance absorption of visible light. Moreover, the absorption edge of $ZnFe_2O_4$/MMT K10 nanocomposite was extended to above 750 nm. In addition, the band gaps of $ZnFe_2O_4$ and $ZnFe_2O_4$/MMT K10 nanocomposite was calculated from the Kubelka–Munk function, as shown in Fig. 4b. As, expected band gaps of $ZnFe_2O_4$ and $ZnFe_2O_4$/MMT K10 nanocomposite was measured to be about 2.04 eV and 1.98 eV, respectively.

The magnetic property of the obtained samples was investigated using a vibrating sample magnetometer (VSM). Fig. 5 shows the room-temperature magnetization hysteresis loops of the $ZnFe_2O_4$/MMT K10 nanocomposite and pure $ZnFe_2O_4$. The saturation magnetization of the $ZnFe_2O_4$/MMT K10 nanocomposite is 39.6 emu/g, which is lower than that of pure $ZnFe_2O_4$ (67.4 emu/g), mainly attributing to the presence of exfoliated MMT K10 clay. The both samples exhibited a typical hysteresis loop in their magnetic behaviour, indicating that both are soft and strong magnetic materials. The coercivity values obtained for the $ZnFe_2O_4$ and $ZnFe_2O_4$/MMT K10 magnetic materials are 22.8 and 67.3 Oe (inset left top Fig. 5). The results suggest that the $ZnFe_2O_4$/MMT K10

nanocomposite could be easily collected by an external magnetic field after being used (inset right bottom Fig. 5).

The adsorption mechanism of MB can be explained based on the pH-dependent Zeta potential analyses of $ZnFe_2O_4$ and $ZnFe_2O_4$/MMT K10 nanocomposite as shown in Fig. S1. The isoelectric charge (pzc) of $ZnFe_2O_4$ and $ZnFe_2O_4$/MMT K10 nanocomposite were 5.01 and 4.45, respectively. The surface charge (Zeta potential) of $ZnFe_2O_4$/MMT K10 nanocomposite showed positive values at lower pH due to the protonation of surface functional groups and turned negative at higher pH due to deprotonation. Therefore, the surface of $ZnFe_2O_4$/MMT K10 nanocomposite was deprotonated at higher pH and became negatively charged receptors and electrostatically attracts more number of positively charged MB. As evidenced by surface Zeta potential, the negative surface charges of MMT K10 and $ZnFe_2O_4$/MMT K10 nanocomposite (Fig. S1) ensures the efficient adsorption of positively charged cationic. Their positive charges were concentrated on their sulphur (S) or nitrogen (N) atoms [48]. Hence, electrostatic interaction plays a key role in determining adsorption between $ZnFe_2O_4$/MMT K10 nanocomposite and cationic MB molecules. Also, with increasing initial pH, electrostatic forces are formed between the adsorbent surface and the dye molecules, which is due to the electrons present in the adsorbent surface and the cationic MB dye. Such reports have been presented in previous studies [49, 50].

3.3. Adsorption isotherms studies

Adsorption isotherms provide valuable information about adsorption behaviour, surface properties and affinity of the dye toward the adsorbent. Fig. 6 shows the adsorption capacities of $ZnFe_2O_4$/MMT K10 nanocomposite were determined by conducting the adsorption experiment using different initial concentrations (25, 50, 75, 100, 250, 500, 750, and 1000 mg L^{-1}) of MB aqueous solutions at room temperature, and results were compared with bare $ZnFe_2O_4$ nanoparticles. After the adsorption equilibrium, the concentration of remaining MB dye solution was obtained from UV-Vis analysis (Fig. 6) with 100 time dilution. The adsorption capacity was increased with increasing the

concentration of dye solution due to the ascribed to the extent of a driving force of concentration gradients with the increase in the dye concentration. The amount of dye adsorbed on the nanocomposite surface and the amount of dye remaining in the solution at a fixed pH can be evaluated by isotherms [51]. The equilibrium adsorption of the $ZnFe_2O_4$/MMT K10 nanocomposite was analyzed using Langmuir and Freundlich adsorption isotherms [52].

The Langmuir isotherm assumes that the monolayer of dye molecules is adsorbed at definite homogeneous sites on the surface of the adsorbent and that these sites cannot be further occupied by another dye molecule. The linear (Eq. (3)) and non-linear (Eq. (4)) forms of Langmuirequation [53]can be represented as follows:

$$\frac{C_e}{q_e} = \frac{1}{K_L} + \frac{C_e}{q_{max}} \qquad (Eq.3)$$

$$q_e = q_{max}\frac{K_L C_e}{1 + K_L C_e} \qquad (Eq.4)$$

where q_e (mg g^{-1}) and q_{max} (mg g^{-1}) denotes the equilibrium and maximum monolayer adsorption capacity, respectively, and K_L is the Langmuir constant.

The Freundlich adsorption isotherm assumes that dye adsorption takes place at heterogeneous sites on the surface of the adsorbent and that the adsorption capacity of an adsorbent depends on the concentration of the dye. The Freundlich isotherm [54]can be written as follows (Eq. (5) and (6)):

$$\ln q_e = \ln K_F + \frac{\ln C_e}{n} (Eq.5)$$

$$q_e = K_F C_e^{\frac{1}{n}} \qquad (Eq.6)$$

where K_F is the Freundlich constant which signifies the binding energy correlation between the adsorbate and the adsorbent, and n is the measure of the intensity of adsorption.

Non-linear Langmuir and Freundlich isotherm models were fitted with experimental data using Eqs (4) and (6) and then the isotherm constants and correlation factors were calculated. From the experiments data and isotherm analyses revealed that $ZnFe_2O_4$/MMT K10 nanocomposite demonstrated the maximum adsorption capacities of 218.3 mg g^{-1} (Fig. 6) for MB. These values are higher than those

of $ZnFe_2O_4$ (106.2 mg g^{-1}) under the same experimental conditions.The comparison result indicates that the relationship between MMT K10 and $ZnFe_2O_4$ is not just a simple mix. As discussed by XRD and EDAX, the $ZnFe_2O_4$ nanoparticles has successfully intercalated into the silicate layer of MMT K10 and also fully attached on the surface of MMT K10 layer, which further enhanced the adsorption capacity. Overall, $ZnFe_2O_4$ not only used for the magnetic separation, but also paid in attention for the higher adsorption capacity. This result implies that monolayer adsorption took place over the $ZnFe_2O_4$/MMT K10 nanocomposite due to the presence of different anions such as O^- and OH^- [55, 56].

Fig. S2a-d shows the linear plots of Langmuir and Freundlich isotherms for $ZnFe_2O_4$ and $ZnFe_2O_4$/MMT K10 nanocomposite. The Langmuir isotherm constants, maximum adsorption capacity and correlation factors were obtained by the plots of $1/q_e$ vs $1/C_e$ and they are listed in Table 1. Parameters for the linear Freundlich isotherm are also shown in Table 1, where the high values for the correlation coefficient indicated that the experimental data were well correlated by the Langmuir model. The maximum adsorption capacity values are nearly consistent with the experimental data. A high adsorption capacity indicates that good coverage of cationic dyes over the adsorbent surface could be due to the more negatively charged adsorption sites.

3.4 Adsorption kinetics studies

The adsorption kinetics of $ZnFe_2O_4$ and $ZnFe_2O_4$/MMT K10 nanocomposite(Fig. 7) were explored to find their adsorption rates and time required to complete process towards MB adsorption experiments for different contact times at room temperature. After that, the concentration was measured via UV–Vis analysis after diluting the solution 100 times(Fig. S3). The results show that $ZnFe_2O_4$/MMT K10 nanocomposite removed MB with rapid kinetics at the initial contact period and reached adsorption equilibrium at ~40 min due to the presence of high surface area and active sites of the adsorbents. The two of the well-known kinetic models were used to model the experimental data of MB adsorption onto $ZnFe_2O_4$/MMT K10 nanocomposite. Adsorption kinetics was explored by pseudo-first-order and pseudo-second-order models [57].

Pseudo-first-order kinetics explainsrate-determining steps such as chemical reactions and mass transportprocesses which can be expressed (Eq. (7)) as follows:

$$\frac{dq_t}{dt} = K_1(q_e - q_t) \qquad (Eq.7)$$

where q_e (mg g^{-1}) and q_t (mg g^{-1}) denotes the adsorption capacity at equilibrium time and time t (min), respectively, and k1 (g mg^{-1} min^{-1}) isthe pseudo-first-order rate constant. By substituting the boundary conditions(t = 0 to t and qt = 0 to q_t), Eq. (7) can be written as follows:

$$\ln(q_e - q_t) = \ln q_e - k_1\, t \qquad (Eq.8)$$

Pseudo-second-order model that assumes the overall adsorption rateof adsorbate by an adsorbent as chemisorption is represented by thefollowing expression:

$$\frac{dq_t}{d_t} = K_2(q_e - q_t)^2 \qquad (Eq.9)$$

$$\frac{t}{q_t} = \left[\frac{1}{K_2 q_e^2}\right] + \frac{1}{q_e}\, t \qquad (Eq.10)$$

where q_e (mg g^{-1}), and q_t (mg g^{-1}) are the adsorption capacity at theequilibrium time, and time (t), respectively, and k_2 (g mg^{-1} min^{-1})represents the second-order rate constant.

From the experimental data, the kinetic parameters (Table 2) are obtained using the slope and intercept of the linear plots of "ln (q_e-q_t) vs. t" for pseudo first-order and "t/q_t vs. t" for pseudo second-order. Pseudo-first-order kinetic plots did not fit the experimental data well for MB adsorptions by $ZnFe_2O_4$ and $ZnFe_2O_4$/MMT K10 nanocomposite (Fig. 8a&c). Also, the correlation factors for pseudo-first-order kinetic plots were less than 0.8593, whereas pseudo-second-order kinetic plots exhibited correlation factors about 0.9995 for MB dyes used in the experiment (Fig.8d). Pseudo-second-order rate constants were calculated to be 0.0009 g mg^{-1} min^{-1}, under experimental conditions.

The $ZnFe_2O_4$/MMT K10 nanocomposite followed the pseudo-second-order kinetic model for MB dye adsorption. This suggests that adsorption could be dominated by chemisorption rather than physical adsorption. Chemisorption could be a result of ionic interactions with the negatively charged

surface of the $ZnFe_2O_4$/MMT K10 nanocomposite. The maximum adsorption capacities obtained by pseudo-second-order fittings at the concentration of MB (200 mg L^{-1}) were 162.8 mg $g^{-1}$for $ZnFe_2O_4$/MMT K10 nanocomposite, which are very close to our experimental results (163.5 mg g^{-1}). Kinetic studies on $ZnFe_2O_4$ shows the similar adsorption behaviours (Figs. 8b). The more negative functional groups and excellent adsorption sites may reveal the rapid adsorption of MB by $ZnFe_2O_4$/MMT K10 nanocomposite.

3.5. Mechanism of MB adsorptions

FT-IR analysis was performed to determine the mechanism for adsorption of dye on the surface of the $ZnFe_2O_4$/MMT K10 nanocomposite. Fig.S4 shows the FT-IR spectra of MB after being adsorbed on the surface of the $ZnFe_2O_4$/MMT K10 nanocomposite. Before adsorption, the surface of the $ZnFe_2O_4$/MMT K10 nanocomposite has characteristic peaks at 590 and 420 cm^{-1}, 1726 and 1628 cm^{-1}, 528 and 468 cm^{-1} corresponds to the Zn−O, C=O and Si− O, respectively. After dye adsorption, a new peak at around 1593 cm^{-1} distinctly appeared and a more broadened peak was observed. This peak can be assigned to the vibration of the aromatic ring owing to the C=C bond, indicating that the dyes are attached on the $ZnFe_2O_4$/MMT K10 nanocomposite surface. Also, small peak shift was observed in the $ZnFe_2O_4$/MMT K10 nanocomposite after dye adsorption. This peak shift is attributed to the electrostatic interactions between cationic dyes and the negatively charged surface of the $ZnFe_2O_4$/MMT K10 nanocomposite. This behaviour has been supported by zeta potential analysis. The zeta potential of the $ZnFe_2O_4$/MMT K10 nanocomposite was −32.5 mV at the experimental pH, indicating good emulsion stability and dispersion. This also confirms that the surface of the nanocomposite becomes more negatively charged than those of pristine $ZnFe_2O_4$ due to the presence MMT K10 clay. This negatively charged surface can actively adsorb cationic dyes, which improved the dye adsorption capacity of the $ZnFe_2O_4$/MMT K10 nanocomposite. Based on this, different types of possible molecular interactions over the surface of $ZnFe_2O_4$/MMT K10 nanocomposite with cationic dyes are illustrated in Fig. 9. Generally, the $ZnFe_2O_4$/MMT K10 nanocomposite was strongly bound

with the dye molecules through hydrogen bonding and electrostatic interactions with the MMT K10 clay and the nanofibrous, resulting in rapid cationic dye adsorption.

3.6. Adsorbent recycles studies

The photo-induced recycling capability and stability of $ZnFe_2O_4$/MMT K10 nanocomposite were tested repeatedly five times through adsorption-desorption cycles. The photo-induced recycling properties of nanocomposite were investigated in the presence of natural sun light as shown in Fig. 10. After batch adsorption experiments, the $ZnFe_2O_4$/MMT K10 nanocomposite were collected using an external magnet and dispersed well with de-ionized water and followed by irradiation the natural sun light for 180 min with shadow. After the irradiation, adsorbent was collected with magnet and vacuum drying at 80 °C before proceeds the next batch adsorption experiment with the same experimental conditions. The adsorption capacity of $ZnFe_2O_4$/MMT K10 nanocomposite was above 97% after five cycles (Fig. 11). The results revealed that $ZnFe_2O_4$/MMT K10 nanocomposite could be effectively degrade the MB under sun light irradiation in recycling process. So we believe that the photo-induced regeneration method can be avoiding the secondary pollutant by solvent extraction.

4. Conclusion

In summary, the stacked layer structure of $ZnFe_2O_4$/MMT K10 nanocomposite was successfully synthesized and utilized as the adsorbent for the removal of MB dye from aqueous solutions. The batch adsorption experiments were carried out to determine the adsorption capacities of $ZnFe_2O_4$/MMT K10 nanocomposite towards MB and the data were systematically evaluated using Langmuir and Freundlich isotherm models which revealed that the Langmuir isotherm was fitted well. Moreover, $ZnFe_2O_4$/MMT K10 nanocomposite showed maximum adsorption capacities of 218.3 mg g^{-1} for MB. This value is significantly greater than those of bare $ZnFe_2O_4$. $ZnFe_2O_4$/MMT K10 nanocomposite also showed rapid MB adsorption kinetics and attained equilibrium within 40 min. We believe the high MB adsorption capacities of $ZnFe_2O_4$/MMT K10 nanocomposite are due to synergistic effects of electrostatic attraction and hydrogen bonding between the functional groups of $ZnFe_2O_4$/MMT K10 nanocomposite and lone-

pair electrons of the N group of MB. In addition, the $ZnFe_2O_4$/MMT K10 nanocomposite has proven excellent photo-induced recyclability of 97.6% for MB dye after five successful runs. This study is expected to offer the development of magnetic $ZnFe_2O_4$/MMT K10 clay-based adsorbent that effectively removes various cationic dyes from aqueous wastes.

References

[1] A. Bhatnagar, A.K. Jain, A comparative adsorption study with different industrial wastes as adsorbents for removal of cationic dyes from water, J. Colloid Interface Sci. 281 (2005) 49–55.

[2] J.W. Lee, S.P. Choi, R. Thiruvenkatachari, W.G. Shim, H. Moon, Evaluation of the Performance of Adsorption and Coagulation Processes for the Maximum Removal of Reactive Dyes. Dyes Pigm. 69 (2006) 196−203.

[3] C. Li, H. Zhong, S. Wang, J. Xue, Z. Zhang, Removal of Basic Dye (Methylene Blue) from Aqueous Solution Using Zeolite Synthesized from Electrolytic Manganese Residue. J. Ind. Eng. Chem. 23 (2015) 344−352.

[4] Z. Carmen, S. Daniel, Textile Organic Dyes烜Characteristics, Polluting Effects and separation/Elimination Procedures from Industrial Effluents − A Critical Overview. Organic Pollutants Ten Years after the Stockholm Convention, Environmental and Analytical Update; InTech, 2012.

[5] M. Chen, T. Shang, W. Fang, G. Diao, Study on Adsorption and Desorption Properties of the Starch Grafted P-Tert-Butyl- Calix[n]Arene for Butyl Rhodamine B Solution. J. Hazard. Mater. 185 (2011) 914−921.

[6] A. Akbari, J.C. Remigy, P. Aptel, Treatment of Textile Dye Effluent Using a Polyamide-Based Nanofiltration Membrane. Chem. Eng. Process. 41 (2002) 601−609.

[7] S.S. Moghaddam, M.R. Alavi Moghaddam, M. Arami, Coagulation/Flocculation Process for Dye Removal Using Sludge from Water Treatment Plant: Optimization through Response Surface Methodology. J. Hazard. Mater. 175 (2010) 651−657.

[8] V.K. Gupta, I. Ali, T.A. Saleh, A. Nayak, S. Agarwal, Chemical Treatment Technologies for Waste-Water Recycling – An Overview. RSC Adv. (2012) 6380−6388.

[9] K.H. Gonawala, M.J. Mehta, Removal of Color from Different Dye Wastewater by Using Ferric Oxide as an Adsorbent. Int. J. Eng. Res. Ind. Appl. 4 (2014) 102.

[10] S.A. Nabi, M. Shahadat, R. Bushra, A.H Shalla, F. Ahmed, Development of Composite Ion-Exchange Adsorbent for Pollutants Removal from Environmental Wastes. Chem. Eng. J. 165 (2010) 405−412.

[11] Y. Sun, G. Wang, Q. Dong, B. Qian, Y. Meng, J. Qiu, Electrolysis Removal of Methyl Orange Dye from Water by Electrospun Activated Carbon Fibers Modified with Carbon Nanotubes. Chem. Eng. J. 253 (2014) 73−77.

[12] M.X. Zhu, L. Lee, H.H. Wang, Z. Wang, Removal of an Anionic Dye by Adsorption/Precipitation Processes Using Alkaline White Mud. J. Hazard. Mater. 149 (2007) 735−741.

[13] L. Kashinath, K. Namratha, S. Srikantaswamy, A. Vinu, K. Byrappa, Microwave Treated Sol−Gel Synthesis and Characterization of Hybrid ZnS−RGO Composites for Efficient Photodegradation of Dyes. New J. Chem. 41 (2017) 1723−1735.

[14] C. Fritzmann, J. Löwenberg, T. Wintgens, T. Melin, State-of the- Art of Reverse Osmosis Desalination. Desalination 216 (2007) 1−76.

[15] D. Mahanta, G. Madras, S. Radhakrishnan, S. Patil, Adsorption of sulfonated dyes by polyaniline emeraldine salt and its kinetics, J. Phys. Chem. B 112 (2008) 10153–10157.

[16] L. Lian, L. Guo, C. Guo, Adsorption of Congo red from aqueous solutions onto Cabentonite, J. Hazard. Mater. 161 (2009) 126–131.

[17] P. Pendleton, S.H. Wu, Kinetics of dodecanoic acid adsorption from caustic solution by activated carbon, J. Colloid Interface Sci. 226 (2003) 245–250.

[18] A. Faki,M.Turan, O. Ozdemir, A.Z. Turan, Analysis of fixed-bed column adsorption of reactive yellow 176 onto surfactant-modified zeolite, Ind. Eng. Chem. Res. 47 (2008) 6999–7004.

[19] P. Pengthamkeerati, T. Satapanajaru, O. Singchan, Sorption of reactive dye from aqueous solution on biomass fly ash, J. Hazard. Mater. 153 (2008) 1149–1156.

[20] N.K. Lazaridis, G.Z. Kyzas, A.A. Vassiliou, D.N. Bikiaris, Chitosan derivatives as biosorbents for basic dyes, Langmuir 23 (2007) 7634–7643.

[21] F.A. Pavan, A.C. Mazzocato, Y. Gushikem, Removal of methylene blue dye from aqueous solutions by adsorption using yellow passion fruit peel as adsorbent, Bioresource Technol. 99 (2008) 3162–3165.

[22] R.A. Shawabkeh, M.F. Tutunji, Experimental study and modeling of basic dye sorption by diatomaceous clay, Appl. Clay Sci. 24 (2003) 111–120.

[23] A.H. Gemeay, A.S. El-Sherbiny, A.B. Zaki, Adsorption and kinetic studies of the intercalation of some organic compounds onto Na+-montmorillonite, J. Colloid Interface Sci. 245 (2002) 116–125.

[24] A.H. Gemeay, Adsorption characteristics and the kinetics of the cation exchange of rhodamine 6G with Na^{+}-montmorillonite, J. Colloid Interface Sci. 251 (2002) 235–241.

[25] E. Forgacs, T. Cserhati, G. Oros, Removal of Synthetic Dyes from Wastewaters: A Review. Environ. Int. (2004) 953−971.

[26] M. Momina, M. Shahadat, S. Isamil, Regeneration Performance of Clay-Based Adsorbents for the Removal of Industrial Dyes: A Review. RSC Adv. 8 (2018) 24571−24587.

[27] J. Fei, Y. Cui, X. Yan, W. Qi, Y. Yang, K. Wang, Q. He, J. Li, Controlled preparation of MnO_2 hierarchical hollow nanostructures and their application in water treatment, Adv. Mater. 20 (2008) 452–456.

[28] L.S. Zhong, J.S. Hu, H.P. Liang, A.M. Cao, W.G. Song, L.J. Wan, Self-assembled 3D flowerlike iron oxide nanostructures and their application in water treatment, Adv. Mater. 18 (2006) 2426–2431.

[29] V. Belessi, G. Romanos, N. Boukos, D. Lambropoulou, C. Trapalis, Removal of Reactive Red 195 from aqueous solutions by adsorption on the surface of TiO_2 nanoparticles, J. Hazard. Mater. 170 (2009) 836–844.

[30] X. Hou, J. Feng, Y. Ren, Z.nFan,, M. Zhang, Synthesis and adsorption properties of spongelike porous $MnFe_2O_4$, Colloids Surf. A 363 (2010) 1–7.

[31] L. Wang, J. Li, Y. Wang, L. Zhao, Q. Jiang, Adsorption capability for Congo red on nanocrystalline MFe_2O_4 (M = Mn, Fe, Co,Ni) spinel ferrites, Chemical Engineering Journal 181–182 (2012) 72– 79.

[32] A. Ngomsik, A. Bee,M.Draye, G. Cote, V. Cabuil, Magnetic nano and microparticles for metal removal and environmental applications: a review, C. R. Chimie. 8 (2005) 963–970.

[33] S. Qu, F. Huang, S. Yu, G. Chen, J. Kong, Magnetic removal of dyes from aqueous solution using multi-walled carbon nanotubes filled with Fe_2O_3 particles, J. Hazard. Mater. 160 (2008) 643–647.

[34] J.L. Gong, B. Wang, G.M. Zeng, C.P. Yang, C.G. Niu, Q.Y. Niu, W.J. Zhou, Y. Liang, Removal of cationic dyes from aqueous solution using magnetic multi-wall carbon nanotube nanocomposite as adsorbent, J. Hazard. Mater. 164 (2009) 1517–1522.

[35] N. Yang, S. Zhu, D. Zhang, S. Xu, Synthesis and properties of magnetic Fe_3O_4- activated carbon nanocomposite particles for dye removal, Mater. Lett. 62 (2008) 645–647.

[36] T. Xie, L. Xu, C. Liu, Y. Wang, Magnetic composite $ZnFe_2O_4/SrFe_{12}O_{19}$: Preparation, characterization, and photocatalytic activity under visible light, Applied Surface Science 273 (2013) 684-691.

[37]Zhang, P., Xiang, M., Liu, H., Yang, C., Deng, S., 2019. Novel two-dimensional magnetic titanium carbide for methylene blue removal over a wide pH range: Insight into removal performance and mechanism. ACS Appl. Mater.Interf. 11(27), 24027-24036.

[38] C. Aruljothi, P. Manivel, T. Vasuki, Reduced graphene oxide wrapped $ZnFe_2O_4$ nanospheres as selective magnetically recyclable Photocatalysts under visible light irradiation, Carbon Letters, 32 (2022) 1703–1714.

[39] K. Y Nandiwale, P. S Niphadkar, V. V Bokade, Synthesis of Oxygenated Fuel Additives via Acetylation of Bio-Glycerol over H_2SO_4 Modified Montmorillonite K10 Catalyst, Prog. Petrochemical Sci. 1 (2018).

[40] S. Bhandari and V. Kasana, Fe^{3+-} montmorillonite K10 as an efficient, green and reusable heterogeneous catalyst for synthesis of mannich type reaction under solvent-free condition. Int Res J Pure Appl Chem 16 (2018) 1–11.

[41] A. Marsh, A. Heath, P. Patureau, M. Evernden, P. Walker, Alkali activation behaviour of un-calcined montmorillonite and illite clay minerals. Appl Clay Sci 166 (2018) 250–261.

[42] S.M. Lee and D. Tiwari, Organo and inorgano-organo-modified clays in the remediation of aqueous solutions: an overview. Appl. Clay Sci. 59–60 (2012) 84–102.

[43] O.A. Oyetade, V.O. Nyamori, B.S. Martincigh, S.B. Jonnalagadda, Effectiveness of Carbon Nanotube−Cobalt Ferrite Nanocomposites for the Adsorption of Rhodamine B from Aqueous Solutions. RSC Adv. 5 (2015) 22724−22739.

[44] S. Yavari, N.M. Mahmodi, P. Teymouri, B. Shahmoradi, A. Maleki, Cobalt Ferrite Nanoparticles: Preparation, Characterization and Anionic Dye Removal Capability. J. Taiwan Inst. Chem. Eng. 59 (2016) 320−329.

[45] M. Hajjaji and H.E. Arfaoui, Adsorption of methylene blue and zinc ions on raw and acid-activated bentonite from Morocco. Appl. Clay Sci. 46 (2009) 418–421.

[46] L.M. Wu, C.H. Zhou, D.S. Tong, W.H. Yu, Novel hydrothermal carbonization of cellulose catalyzed by montmorillonite to produce kerogen-like hydrochar. Cellulose 21 (2014) 2845–2857.

[47] A.M. Jubb, and H.C Allen, Vibrational spectroscopic characterization of hematite, maghemite, and magnetite thin films produced by vapor deposition. ACS Appl Mater Interfaces 2 (2010) 2804–2812.

[48] N.M. Tran, Q.T.H. Ta, A. Sreedhar, J.S. Noh, Ti3C2Tx MXene playing as a strong methylene blue adsorbent in wastewater. Appl. Surf. Sci. 537 (2021) 148006.

[49] P. Kar, S. Sardar, B. Liu, M. Sreemany, P. Lemmens, S. Ghosh, S.K. Pal, Facile synthesis of reduced graphene oxide–gold nanohybrid for potential use in industrial waste-water treatment, Sci. Technol. Adv. Mater. 17 (2016) 375–386.

[50] M.J. Hwang, M.G. Kim, S. Kim, Y.C. Kim, H.W. Seo, J.K. Cho, I.K. Park, J. Suhr, H. Moon, J.C. Koo, Cathodic electrophoretic deposition (EPD) of phenylenediamine-modified graphene oxide (GO) for anti-corrosion protection of metal surfaces, Carbon 142 (2019) 68–77.

[51] L. Mouni, L. Belkhiri, J.C. Bollinger, A. Bouzaza, A. Assadi, A. Tirri, F. Dahmoune, K. Madani, H. Remini, Removal of Methylene Blue from Aqueous Solutions by Adsorption on Kaolin: Kinetic and Equilibrium Studies. Appl. Clay Sci. 153 (2018) 38−45.

[52] Langmuir, I. The Constitution and Fundamental Properties of Solids and Liquids. Part I. Solids. J. Am. Chem. Soc. 1916, 38, 2221−2295.

[53] Limousin, G.; Gaudet, J.-P.; Charlet, L.; Szenknect, S.; Barthès, V.; Krimissa, M. Sorption Isotherms: A Review on Physical Bases, Modeling and Measurement. Appl. Geochem. 2007, 22, 249−275.

[54] Ai, L.; Zhou, Y.; Jiang, J. Removal of Methylene Blue from Aqueous Solution by Montmorillonite/CoFe2O4 Composite with Magnetic Separation Performance. Desalination 2011, 266, 72−77.

[55] Chandra Kanth P, Maitrayee U. Trivedi, Khushali Patel, Nirendra M. Misra, and Manoj Kumar Pandey, Cucurbituril-Functionalized Nanocomposite as a Promising Industrial Adsorbent for Rapid Cationic Dye Removal, ACS Omega 2021, 6, 3024−3036.

[56] R. Foroutan, R. Mohammadi, F. MousaKhanloo, S. Sahebi, B. Ramavandi, P. Senthil Kumar, K. H. Vardhan, Performance of montmorillonite/graphene oxide/$CoFe_2O_4$ as a magnetic and recyclable nanocomposite for cleaning methyl violet dye-laden wastewater, Advanced Powder Technology 31 (2020) 3993–4004.

[57] Li, K., Zou, G., Jiao, T., Xing, R., Zhang, L., Zhou, J., Zhang, Q., Peng, Q., 2018. SelfassembledMXene-based nanocomposites via layer-by-layer strategy for elevated adsorption capacities. Colloid. Surface. Physicochem. Eng. Aspect. 553, 105–113.

[58] Y. Fu Y and X Wang, Magnetically Separable $ZnFe_2O_4$–Graphene Catalyst and its High Photocatalytic Performance under Visible Light Irradiation. Ind. Eng. Chem. Res. 50 (2011) 7210-7218.

Figures

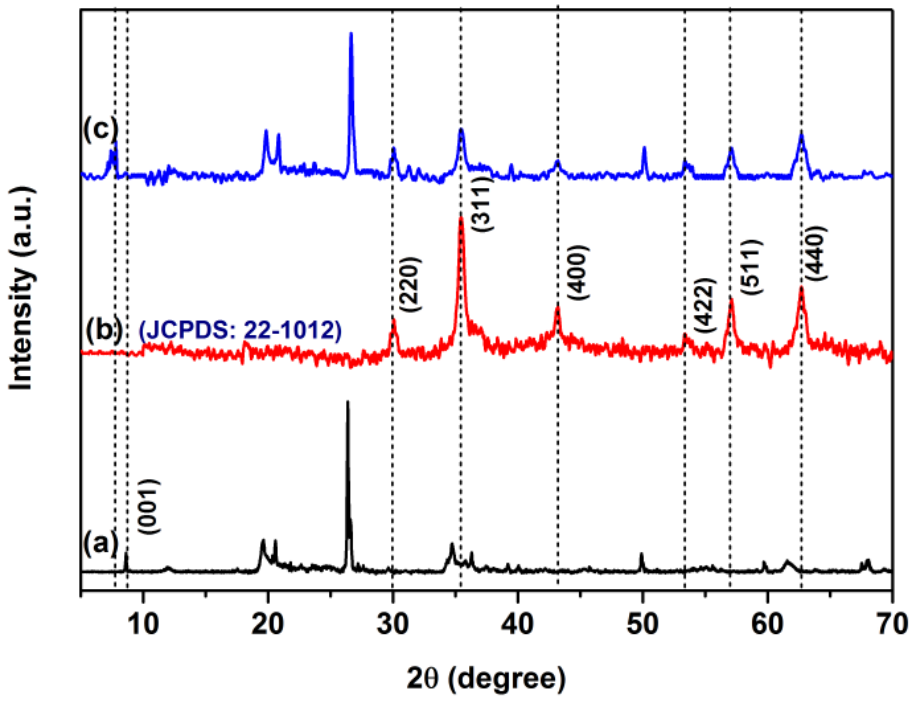

Figure 1. X-ray diffraction patterns of (a) MMT K10, (b) $ZnFe_2O_4$ and (c) $ZnFe_2O_4$/MMT K10 nanocomposite

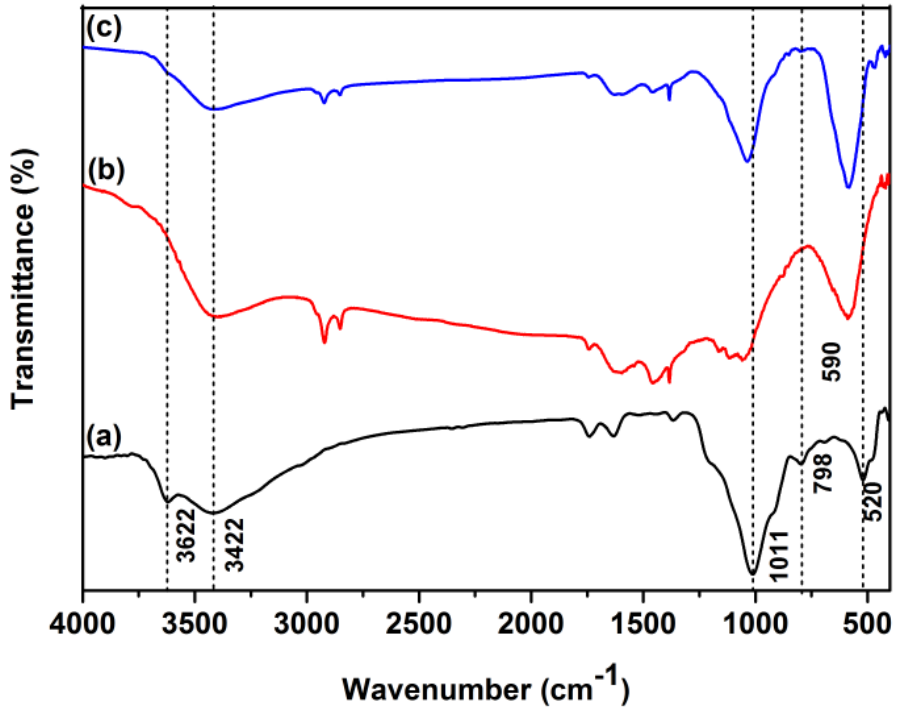

Figure 2 FT-IR spectra of (a) MMT K10 clay, (b) $ZnFe_2O_4$ and (c) $ZnFe_2O_4$/MMT K10 nanocomposite

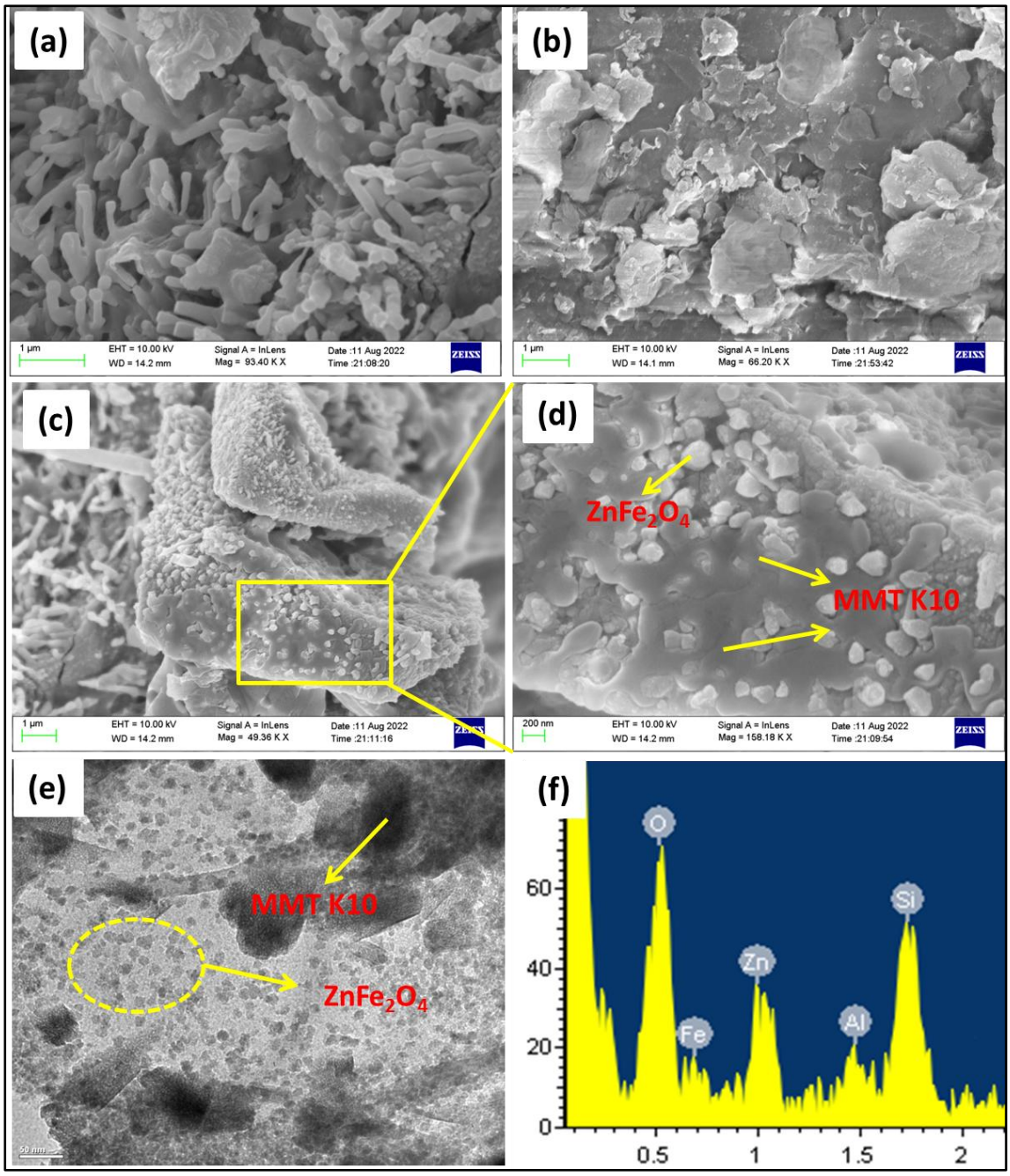

Figure 3. SEM image for (a) $ZnFe_2O_4$, (b) MMT K10 clay, (c&d) $ZnFe_2O_4$/MMT K10 nanocomposite and (e) TEM images of $ZnFe_2O_4$/MMT K10 nanocomposite and (f) EDX analysis of $ZnFe_2O_4$/MMT K10 nanocomposite.

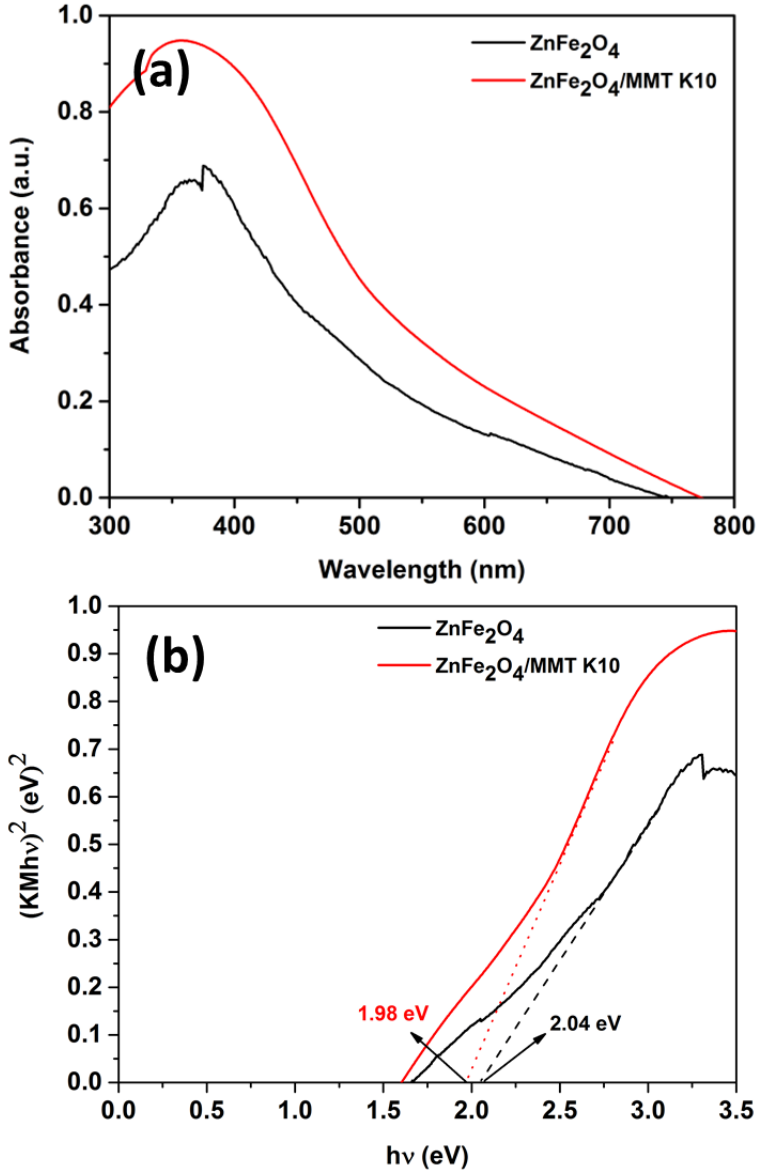

Figure 4. (a) UV-Vis DRS spectra, (b) K-M plot of $ZnFe_2O_4$ and $ZnFe_2O_4$/MMT K10 nanocomposite

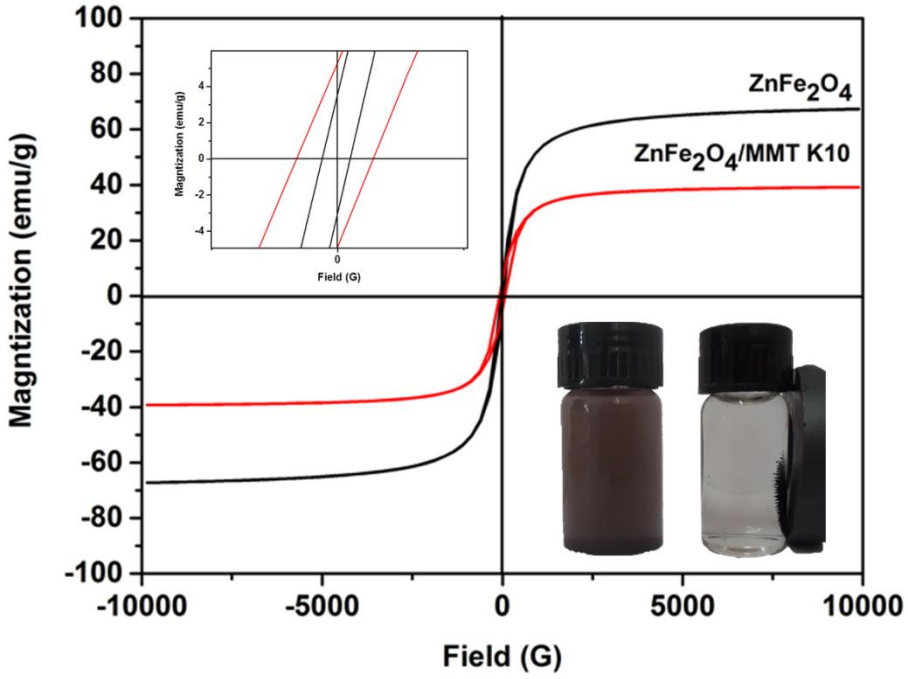

Figure 5. VSM studies of $ZnFe_2O_4$ and $ZnFe_2O_4$/MMT K10 nanocomposite

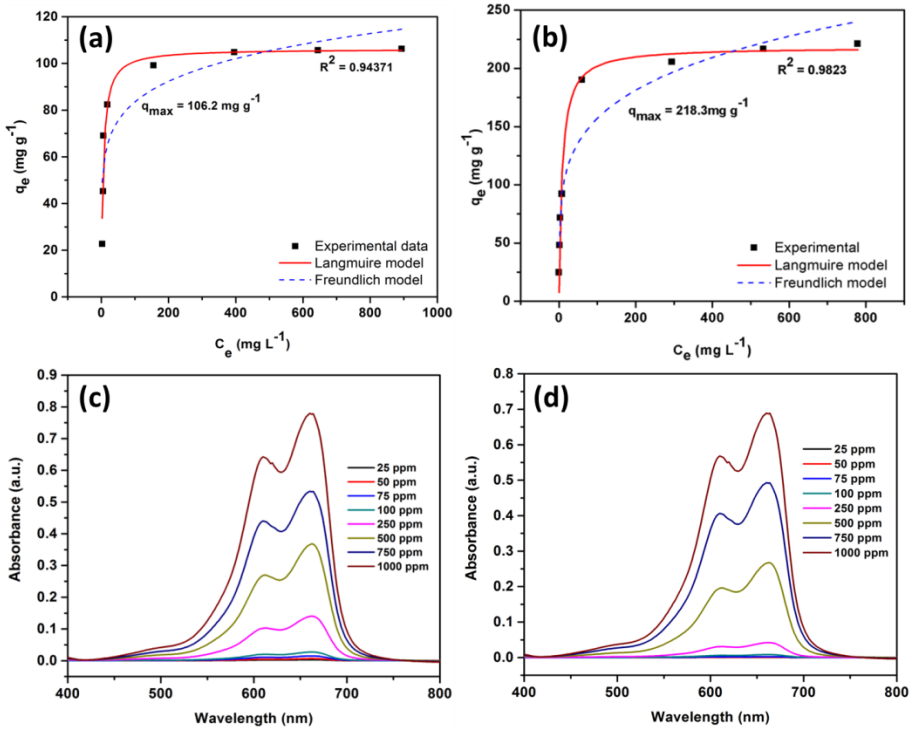

Figure 6. Langmuir and Freundlich isotherms and absorbance studies of MB after equilibrium for (a&c) $ZnFe_2O_4$, (b&d) $ZnFe_2O_4$/MMT K10 nanocomposite.

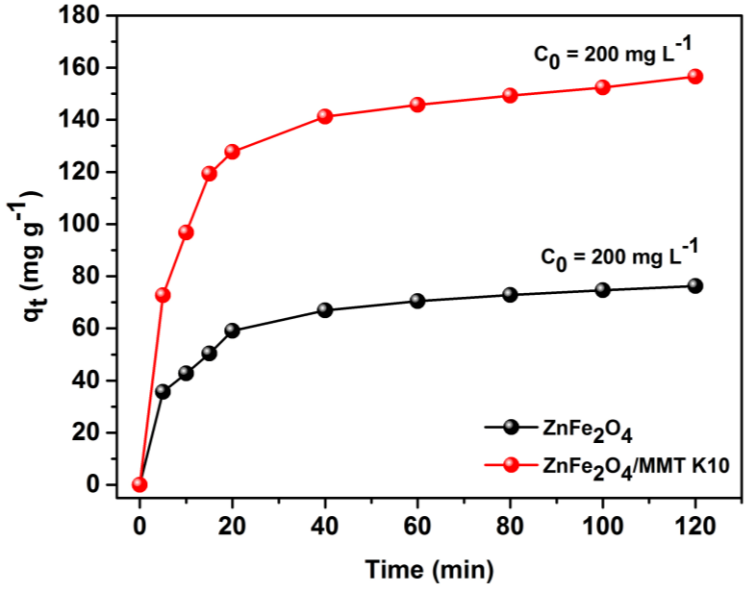

Figure 7. Adsorption kinetics studies of $ZnFe_2O_4$ and $ZnFe_2O_4$/MMT K10 nanocomposite (Initial concentrations of MB = 200 mg L^{-1}).

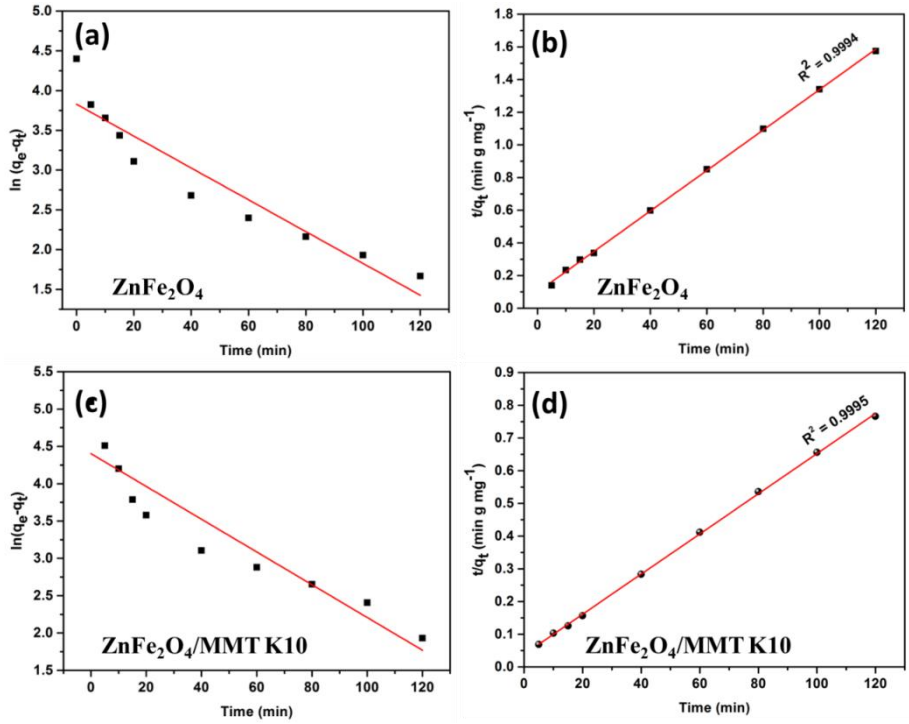

Figure 8. Plot of MB adsorption kinetics using pseudo-first-order (a&c) and pseudo-second-order (b&d) models.

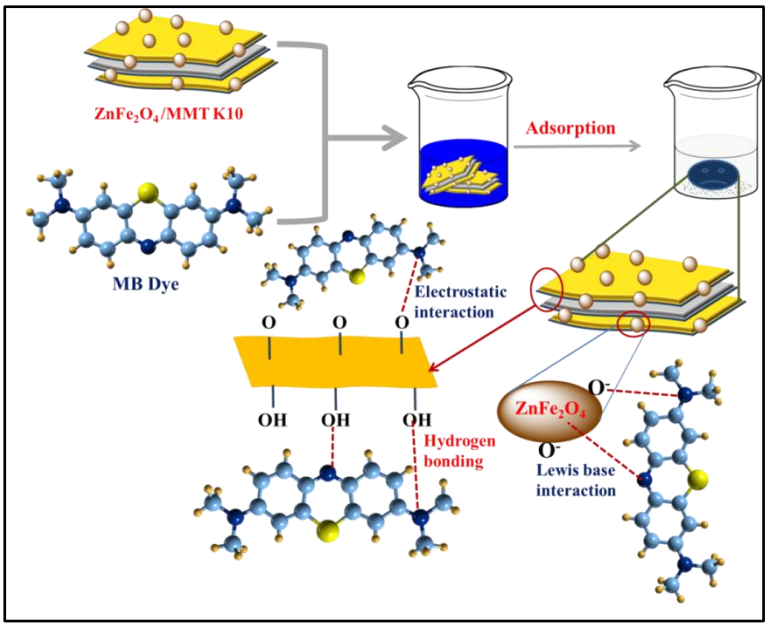

Figure 9. Scheme of plausible mechanism for MB dye adsorption on the $ZnFe_2O_4$/MMT K10 nanocomposite

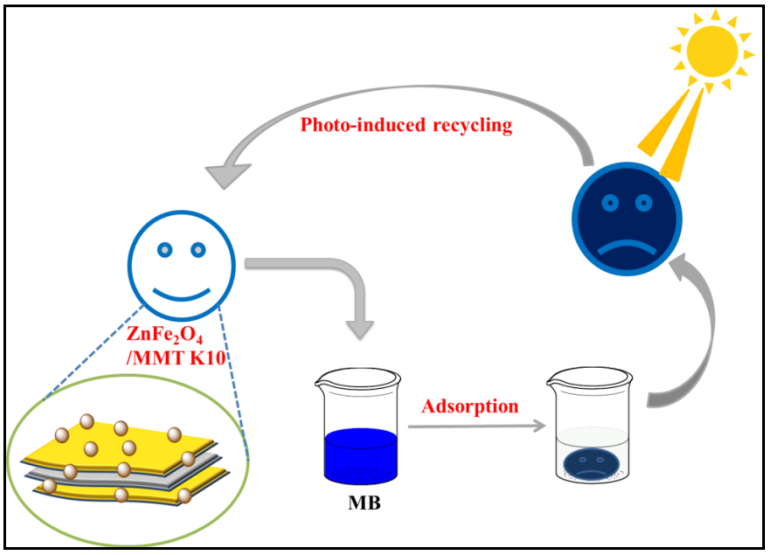

Figure 10. Scheme of dye absorption and photo-induced recycling of the $ZnFe_2O_4$/MMT K10 nanocomposite

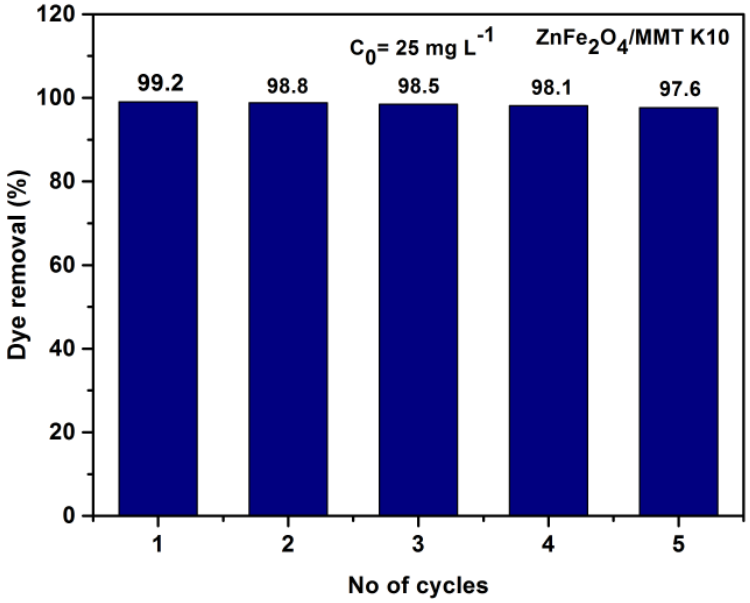

Figure 11. Recycle test of $ZnFe_2O_4$/MMT K10 nanocomposite (MB = 25 mg L^{-1}, reaction time = 180 min).

Table 1. Parameters of the linear Langmuir and Freundlich models for the adsorptions of MB by $ZnFe_2O_4$ and $ZnFe_2O_4$/MMT K10 nanocomposite.

Isotherm	**Parameters**	**$ZnFe_2O_4$**	**$ZnFe_2O_4$/MMT K10**
Langmuir	K_L (L mg^{-1})	0.1043	0.1042
	q_{max}(mg g^{-1})	109.76	212.76
	R^2	0.9968	0.9989
Freundlich	K_F (L mg^{-1})	29.02	35.58
	n	4.64	3.22
	R^2	0.7564	0.8624

Table 2. Kinetic parameters of the pseudo-first-order and pseudo-second-order models for MB adsorptions by $ZnFe_2O_4$ and $ZnFe_2O_4$/MMT K10nanocomposite.

Adsorbent	Pseudo-first-order model			Pseudo-second-order model		
	k_1 (min^{-1})	q_e (mg g^{-1})	R^2	k_2 (g mg^{-1} min^{-1})	q_e (mg g^{-1})	R^2
$ZnFe_2O_4$	0.0001	50	0.8931	0.0015	80.71	0.9994
$ZnFe_2O_4$/MMT K10	0.0001	46.29	0.8593	0.0009	162.86	0.9995